Silicon (2024) 16:3539–3551
https://doi.org/10.1007/s12633-023-02840-6

RESEARCH

Microstructure Study of Friction Stir Processed Hypereutectic Al-20Si Alloy and Analysis of the Wear Behaviour using Machine Learning Algorithms

Mihira Acharya[1] · **Animesh Mandal**[1]

Received: 18 October 2023 / Accepted: 29 December 2023 / Published online: 14 March 2024

Abstract
Al–20Si alloy was subjected to friction stir processing to find its effect on the microstructure and wear behaviour. The microstructures of as-cast and friction stir processed (FSP) alloy were studied using optical microscopy and field emission scanning electron microscopy. The microstructure analysis showed significant refinement of Si particles in Al–20Si alloy by FSP. Similarly, for the experimental study of the wear behaviour, three different parameters: sliding velocity, normal load, and sliding distance were considered. In this study, five different machine learning (ML) algorithms were used for the prediction of wear rate. The hyper parameter tuning of each model was carried out for accurate comparisons. The models were then evaluated on the basis of different statistical metrics to find the superior model. Random Forest model showed the highest prediction accuracy (R2 = 0.8846) and was considered for comparing the wear rates with experimental values.

Keywords Al–20Si · Primary Si · Eutectic Si · Wear · FSP · ML

1 Introduction

Aluminium Silicon alloys are preferred over other alloys because of high strength-to-weight ratio, high castability, high weldability, good corrosion resistance, etc. [1, 2]. Cast aluminum-silicon (Al–Si) alloys that are hypereutectic possess a variety of unique and fascinating properties, including high wear resistance, high strength and hardness, and low thermal expansion coefficients [3]. They are therefore used in various internal combustion engine components such as pistons, cylinder blocks, and compressors which are exposed to severe wear conditions [4, 5] and [6–8]. The frction and wear in the cylinder surace results in reduction of energy efficiency. The poor wear resistance of pure and non-machined aluminium resulted the use of grey cast iron as cylinder liner on the surface of the cylinder [3]. However, the application of grey cast iron leads to the problem of increase in weight and dimensions and thereby decreasing the fuel efficiency [9]. This resulted in considering hypereutectic Al–Si alloy containing hard silicon particles which improves the wear resistance with reduced weight and better fuel efficiency. Previous studies [3–9] show that the wear performance of these alloys is significantly impacted by the Si particle content as well as the morphology, size, and distribution. The fractures which lead to the failure of the material, nucleate at the brittle Si particles [10]. It further initiates the crack at the interface between Si particles and Al matrix and propagates throughout the matrix. The study by Prasad et al. [11] revealed that the coarse Si particles have a greater probability of cracking when subjected to dry sliding conditions. By reducing the size of the coarse primary silicon, mechanical properties, and wear resistance can be enhanced [12]. Eutectic modification, primary Si particle refinement, and α-Al grain refinement are only a few of the chemical techniques utilized to lessen structural flaws and enhance the microstructural features of such alloys [13, 14]. Since wear depends on the surface layer, not the bulk alloy, the surface modification could extend the life of Al–Si alloys [15]. Friction stir processing is performed on the surface to change the microstructure of Si particles to improve the wear resistance of hypereutectic Al–Si alloys [16].

Artificial Intelligence (AI) and data-driven machine learning algorithms are relatively new additions to the field of

✉ Mihira Acharya
ma10@iitbbs.ac.in

[1] School of Minerals, Metallurgical and Materials Engineering, Indian Institute of Technology Bhubaneswar, Argul 752050, Odisha, India

material science [17, 18], despite the fact that other scientific disciplines, such as chemistry, medical science, and biology, have already incorporated these types of algorithms as reliable tools. The recent successes that have been achieved in integrating ML algorithms in material and tribological properties prediction [19] have paved the way for new possibilities in the fields of material science and tribology [20, 21]. Wein et al. used machine learning algorithms to design and fabricate Al-Co-Cr-Cu-Fe-Ni system (high entropy alloys) to improve the hardness [22]. Similarly, Chang et al. designed the composition of Al-Co-Cr-Fe-Mn-Ni based high entropy alloy to obtain optimum hardness [23]. Recent study by Hasan et al. gives a comparison of the predicted wear behaviour of graphene reinforced aluminium metal matrix with experimental results applying different machine learning models [17, 24]. The traditional analysis frequently falls short of showing a universal understanding of tribological behaviour due to the complexity involved with the numerous parameters that characterize friction and wear. This is because traditional analysis focuses on isolated experimental observations. Machine learning algorithms can be trained with experimental tribological data in order to predict the tribological behaviour for various material and tribological variable combinations. Different machine learning algorithms, such as, Random Forest (RF), Gradient Boosting Machine (GBM), Support Vector Regression (SVR), and K-nearest neighbour (KNN) algorithms are capable of recognizing the variability in the data and adjusting their learning process to accurately predict the outcome. This can lead to a deeper comprehension of tribological behaviour.

Although, there are several studies available on the effect of FSP on hypo eutectic Al–Si alloy, only a few works have been carried out on hyper eutectic Al–Si alloy. Therefore, a detailed analysis needs to be conducted to find the effect of FSP on the microstructure and tribological properties of Al–20Si alloy. In the present study, friction stir processing is carried out on the cast Al–20Si alloy to find the microstructural changes and investigate the dry sliding wear behaviour by implementing different machine learning algorithms. The wear tests are conducted by changing different parameters such as, sliding velocity, sliding distance, and normal load applied. Machine learning algorithms are used to build models from the previously available data from the literature. The model developed showing the best accuracy is used to predict the wear rate of Al–20Si alloy by applying it to the experimental data and then compared with the predicted values.

2 Materials and Methods

2.1 Friction Stir Process

In the present investigation, commercially pure aluminium and Al–50Si alloy were added in appropriate proportion in conventional stir casting process for the synthesis of Al–20Si alloy. The composition of the alloys are given in Table 1.

Plates of Al–20Si alloys having a dimension of 100 mm × 100 mm × 8 mm were first prepared by conventional stir casting process. The plates were then friction stir processed (FSP) with an H13 steel tool as shown in Fig. 1.

The tool has a shoulder diameter of 18 mm, a probe length of 4.75 mm, a diameter of 7 mm at the root, and a diameter of 3.5 mm at the pin tip. During the processing, a tool rotation speed of 660 rpm was used, and the traverse speed was kept at 40 mm/min. Optical and field emission scanning electron microscopy (FESEM) were used to carry out the microstructural analysis of the as-cast material as well as the various FSP zones of the alloy. The schematic diagram of the friction stir process is shown in Fig. 2.

2.2 Wear Test

For wear analysis, the samples were taken from the FSP region of the plate. Dry sliding wear tests of the samples were carried out using a pin-on-disc type wear testing machine. The samples were prepared in the form of pins

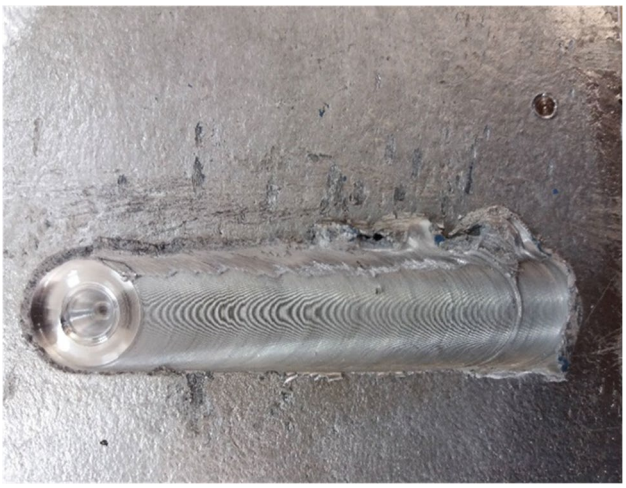

Fig. 1 A typical friction stir processed Al–20Si alloy plate

Table 1 Composition of different elements for the synthesis of Al–20Si alloy

	Al	Si	Fe	Cu	Mg	Mn
CPAL	99.61	0.24	0.12	0.020	0.006	0.004
Al–50Si	50.51	49.22	0.24	0.016	0.008	0.003

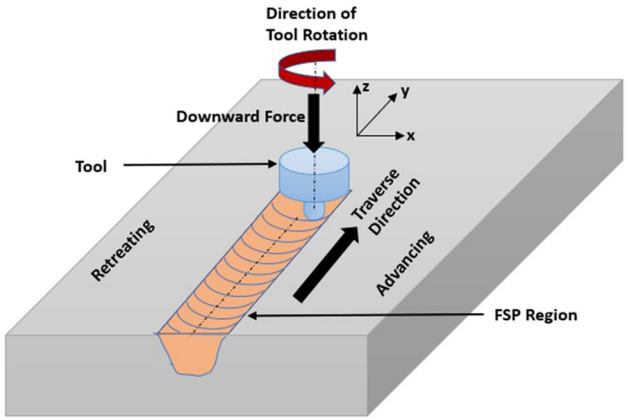

Fig. 2 Schematic Diagram Friction stir process of Al–20Si alloy

according to ASTM G99-05 standard. The faces of the sample pins were polished using SiC grit papers followed by cleaning using acetone solution in an ultrasonic bath. Different wear parameters i.e., normal load, sliding distance, and sliding velocity were varied for the experimental data to be compared with the predicted wear by ML model. The influence of different variables on the wear rate has been discussed in the Section 2.2.1.

2.2.1 Variables Affecting Friction and Wear of Hypereutectic Al-Si Alloys

Effect of Normal Load Previous studies show normal load, sliding velocity and sliding distance have impact on the wear rate [1]. The normal load is considered to be one of the most significant factors in analysing the wear rate of Al–20Si alloy. At lower loading conditions, mild abrasive wear governs the wear behaviour of the alloy. When the load is increased, the contact surfaces are more exposed to the microscale asperities resulting in larger plastic deformation. As a result, the frictional force is enhanced between the dry sliding surfaces and oxides will be formed due to higher heat generation during the process.
Thus, a mechanically mixed layer (MML) will be formed which will decrease the wear rate of the alloy. However, a further increase in load leads to the fracture of this MML and the two sliding surfaces will come into direct contact with each other. Thus, it resulted in severe which is reflected in (Fig. 3).

Effect of Sliding Velocity Sliding velocity also affects the wear rate of Al–20Si alloy. As the sliding velocity is increased, high heat is generated in the sliding surfaces which may lead to the formation of oxides. This layer prevents further loss of material. This leads to a decrease in

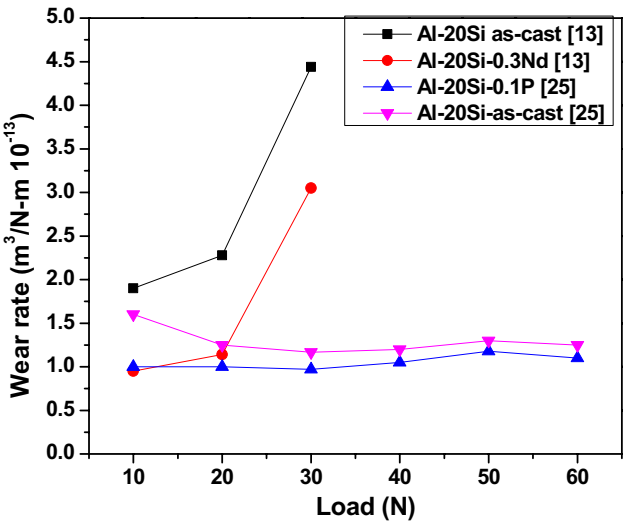

Fig. 3 Effect of load on wear rate in Al–20Si alloy [13, 25]

wear rate by the hard Si particles as the velocity is increased which can be observed in (Fig. 4).

Effect of Sliding Distance Sliding distance also plays important role in the wear behaviour of the alloy. The wear rate is expressed as a function of sliding distance as shown in Fig. 5. The wear rate increases with sliding distance for Al–20Si as can be observed. The increase in wear rate can be attributed to the longer interaction between sample surface and wear track surface [26].

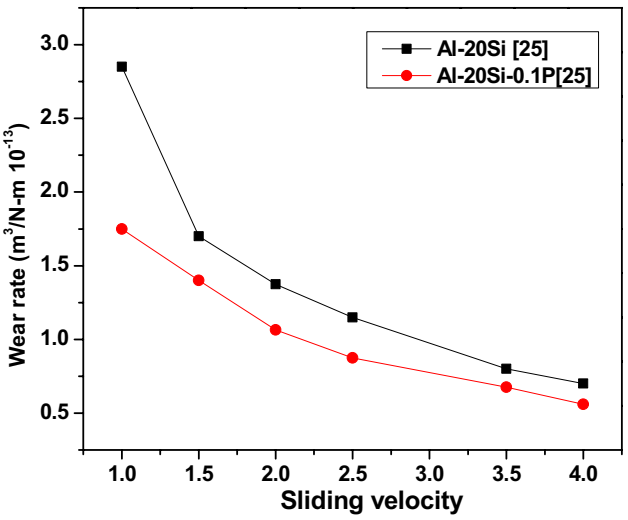

Fig. 4 Effect of sliding velocity on wear rate in Al–20Si alloy [13, 25]

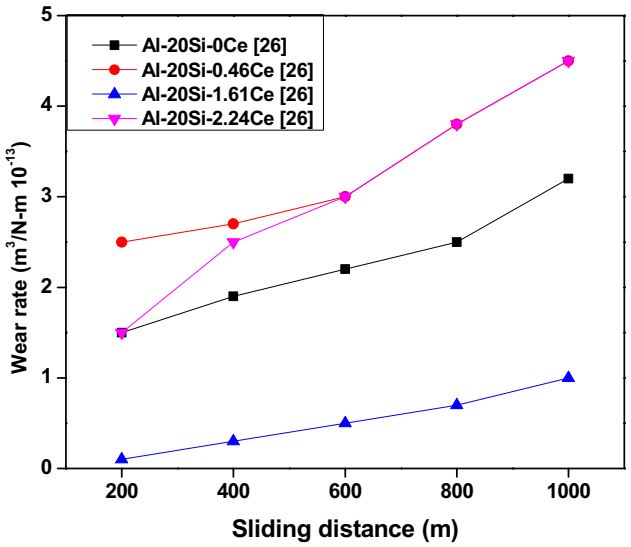

Fig. 5 Effect of sliding distance on wear rate in Al–20Si alloy [26]

2.3 Machine Learning Models

2.3.1 Data Collection

The present study focuses on the prediction of wear rate and primary silicon size of hypereutectic Al–20Si alloy. The dataset for different hypereutectic Al–Si were collected from various sources [1, 13, 25–42]. It included 305 data points from various literatures for building ML models. The variables considered to predict the wear rate are silicon content, tribotesting method, manufacturing process, primary silicon size, Nd, Ce, P, Fe, Ni, Cr, Mg, Cu, hardness, sliding distance, normal load, and speed. Data cleaning, managing missing values, standardisation of data have been applied in the preprocessing steps beore applying different machine learning algorithms.

2.3.2 Description of Different Machine Learning Models Used

The technological advances led to more investigation into the modeling, designing, and enhancing the prediction of different properties and characteristics of alloys over recent years. Different machine learning algorithms have been brought forward to improve the accuracy of predictions in different fields. It is possible to experience a divergence in prediction accuracy due to the fact that every machine learning algorithm has its own individual working principle and applicability. To put it simply, machine learning makes use of pre-programmed algorithms that can acquire and evaluate input data in order to make predictions about output values within a specific domain. When new data is introduced into the algorithms, the algorithms make an attempt to learn and improve their performance by optimizing the functions [33]. This is how intelligence is gradually developed. The following is a description of a selection of well-known ML algorithms that can be applied to the present study.

Random Forest (RF) Random forests are a type of ensemble learning that makes use of a combination of multiple algorithms in order to produce results that are superior for classification and regression. An input is provided at the very top of the "decision tree" that the algorithm uses as its starting point. During the process of learning, the tree develops in proportion to the level of complexity of the data that is being fed into it [26]. Every decision tree has its own unique combination of decision nodes and leaf nodes. Each sample that is provided to the decision nodes is subjected to a test function, which then distributes the sample to the appropriate branch based on the characteristics of the sample. The final output of the model is the average of the outputs of all decision trees.

K-Nearest Neighbour (KNN) K-Nearest Neighbour (KNN) functions through supervised machine learning. It combines historical data patterns with fresh data and seeks to discover novel patterns [43, 44]. The KNN algorithm's goal is to categorise new objects based on their properties and training data. Based on the k training data that are closest to the item, KNN is used to categorize an object. The requirement for the value of k is that it must be odd and greater than one, and that it cannot exceed the quantity of training data.

Gradient Boosting Machine (GBM) Gradient Boosting Machine algorithm uses an ensemble learning approach to create robust forecasting models by integrating several individual regression trees (decision trees) that are considered weak learners. The error rate of models that have been poorly learned can be lowered by using such an algorithm. Weakly learned models show a high bias regarding the training dataset, and have low variance and regularisation [45]. The outputs of these models are considered to be only somewhat improved when compared with arbitrary guesses. These are the characteristics of models that are considered to have been weakly learned. In most cases, boosting algorithms consist of three components: an additive model, weak learners, and a loss function. The operation involves using gradients to determine the limitations of inadequate models. This is accomplished with the aid of an iterative methodology, in which the objective is to finally combine base learners in order to lessen the number of erroneous forecasts, in which decision trees are combined with the assistance of an additive model, all the while using gradient descent to cut down on the loss function.

Support Vector Regression (SVR) A modified version of the support vector machine called the Support Vector Regressor (SVR) is used in regression analysis [17]. To correlate input with desired output measurement and boundaries in SVR,

high-order hyperplanes are developed. These hyperplanes are built using kernel functions like radial basis and linear functions to minimise the generalised error bound. The regularisation parameter and gamma are the two key variables that influence the accuracy of the model when building the hyperplanes. Studies in machine learning and tribology show that SVR models can improve accuracy levels when given high-dimensional data, even when they are capable of working with a limited dataset [24].

ANN (Artificial Neural Network) Model Neural networks, an iterative method, is one of the popular algorithms for examining a variety of data-intensive characteristics, as the foundation for many significant developments in the field of artificial intelligence. ANN regression models are advanced models which consider multi layer perceptrons (MLP) for prediction [46]. In this method, complex nonlinear relationships can be identified and applied similar to the functioning of neurons in the human brain. It consists of three layers: input player, output layer, and hidden layers in between them. These combinedly form a complex network that creates some meaningful output. The network has estimate algorithms that weigh the input parameters according to synaptic activity before calculating the output. This method is able to handle vast amounts of data with enormous covariate spaces by utilising nonlinear mapping functions, which contributes to its robustness and efficiency.

3 Results and Discussion

3.1 Microstructural Analysis

The microstructures of friction stir processed Al–20Si alloy are shown in Fig. 6. The as-cast part portion of the plate which has not undergone the FSP process is shown in Fig. 6a. It contains coarse primary Si particles distributed along with eutectic Si and the α-Al throughout the Al matrix. Figure 6b shows the separating boundary between the microstructure of the as-cast portion and the FSP zone of Al–20Si alloy comprising two regions: as-cast portion and FSP zone Significant refinement of primary Si and modification of eutectic Si in the FSP zone similar to the effect by addition of Sr can be observed in the microstructure.

From the quantitative analysis, the average size of primary Si is reduced from 52.23 µm to 4.69 µm whereas eutectic Si size decreased from 8.12 µm to 0.74 µm. Moreover, both primary and eutectic Si show more uniform distribution in the stir zone of friction stir processed the Al–20Si alloy.

3.2 Mechanism of Refinement of Si Particles in FSP Zone

Friction stir processing results in a significant refinement of coarse primary Si and acicular eutectic Si particles as can be seen in Fig. 7a. Also, the shape factor has been improved which indicates the transformation of Si particles to near spherical shape. The reason for this significant change in the size and morphology of Si particles can be may be due to the exposure to high temperatures and the intense plastic deformation during the process [47]. The fine and near-spherical Si particles are formed because of dynamic recrystallization (DRX) which is influenced by the nucleation and growth during the process [47, 48].

In the case of Al–20Si alloy, the Si particles are non-deformable. During the process of plastic deformation, it is necessary to generate dislocations to accommodate the Si particles that do not deform. When particles are larger than about 0.1 µm in size, zones all around the particles begin to produce highly misoriented cells or subgrains [17, 18]. The size of the particle is directly related to both the size and the misorientation of the deformed zone. Particles having diameter greater than 1 µm are preferred nucleation sites with increased local stored energy [47, 48]. The second-phase particles which are responsible for particle stimulated nucleation thus lead to dynamic recrystallization [18]. According to a report from [49], widely spaced, coarse, and non-deformable Si particles in Al–20Si alloy have the ability to improve DRX through PSN. The size of the Si particles in the alloy satisfies the required condition for PSN mechanism to occur during FSP [50]. It would appear that the Si particles perform

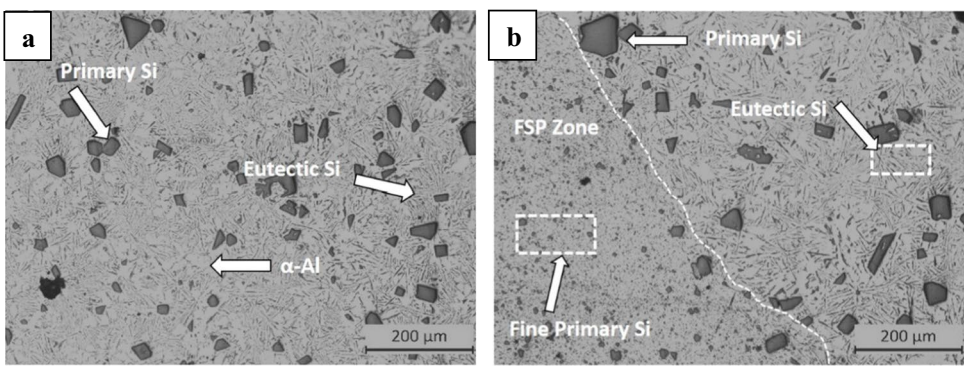

Fig. 6 Optical micrographs of Al–20Si alloy (**a**) as-cast (**b**) containing FSP zone and as-cast region

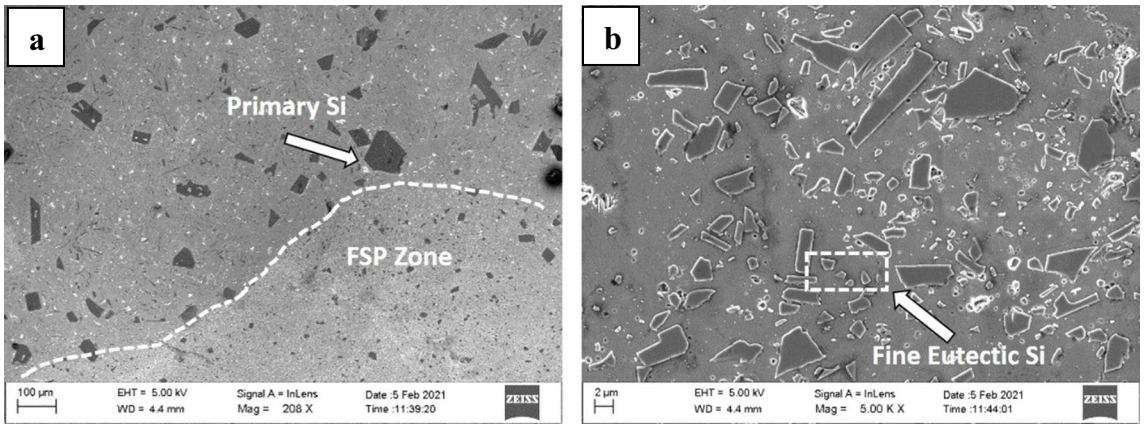

Fig. 7 FESEM micrographs in the FSP zone of Al–20Si alloy (FSP). **a** distribution of primary Si **b** distribution of eutectic Si

the function of nucleation sites for recrystallized grains, which, in conjunction with their high density and uniform distribution, leads to fine grain size. It shows that more in depth-analysis is required in order to determine the mechanism behind the recrystallization in FSP.

3.3 Effect of FSP on Wear Rate

The volumtric wear rate for Al–20Si alloy was 4.7 $(mm^3/m) \times 10^{-5}$ at at sliding distance of 1000 m and sliding velocity of 1.5 m/s. It shows a reduced wear rate of 1.34 $(mm^3/m) \times 10^{-5}$ in the friction stir processed Al–20Si alloy at similar conditions. This can be attributed to the refinement of Si particles during friction stir processing. From Fig. 7, it can be observed that both primary and eutectic Si have a uniform distribution in the matrix with significant refinement. The Si particles are dispersed and oriented in a homogeneous manner throughout the aluminium matrix. This results in improved bonding between the matrix and the Si particles. In addition, the uniform dispersion of Si particles in an aluminium matrix resulted in effective load transmission and thereby reducing the wear rate in the case of friction stir processed Al–20Si alloy as compared to as-cast alloy. Further analysis of the effect of the parameters on the wear rate, different machine learning algorithms were used for the evaluation of wear rate and discussed in detail in subsequent sections.

3.4 Effect of Input Variables on Prediction of Wear Rate

3.4.1 Data Preprocessing

The input variables used here are primary silicon content, tribo-testing method, manufacturing process, primary silicon size, Nd, Ce, P, Fe, Ni, Cr, Mg, Cu, hardness, sliding distance, normal load, and speed. The target variable here is wear rate which has to be predicted using different models. Among these variables, manufacturing process and tribo-testing method are considered categorical variables whereas the rest of the variables are numerical variables. Data preprocessing is the most important step before applying machine learning algorithms to the dataset. The missing values were first checked and replaced with the median fill method in order to get the continuous form of the dataset. The categorical variables were converted to corresponding numerical values. The dataset was then standardized to avoid the effect of the variable having very high values as compared to other variables.

3.4.2 Feature Correlation

After data cleaning and preprocessing, it is to be ensured that data has been properly processed and the correlation among the variables was determined to find the existence of highly correlated variables. Figure 8 shows the correlation among different input variables for the prediction of the wear rate.

From the correlation matrix, it can be observed that Fe, Ni, Cr, Mg, Cu, and Tribo-testing method are highly correlated. Therefore, these variables were removed from the dataset. The new correlations among the remaining variables can be found in the matrix as shown in Fig. 9.

3.5 Prediction of Wear Rate Using Different ML Algorithms

3.5.1 Statistical Evaluation of the Performance of Different ML Models

The performance metrics provide a numerical assessment of how well the machine learning models fit with the actual data.

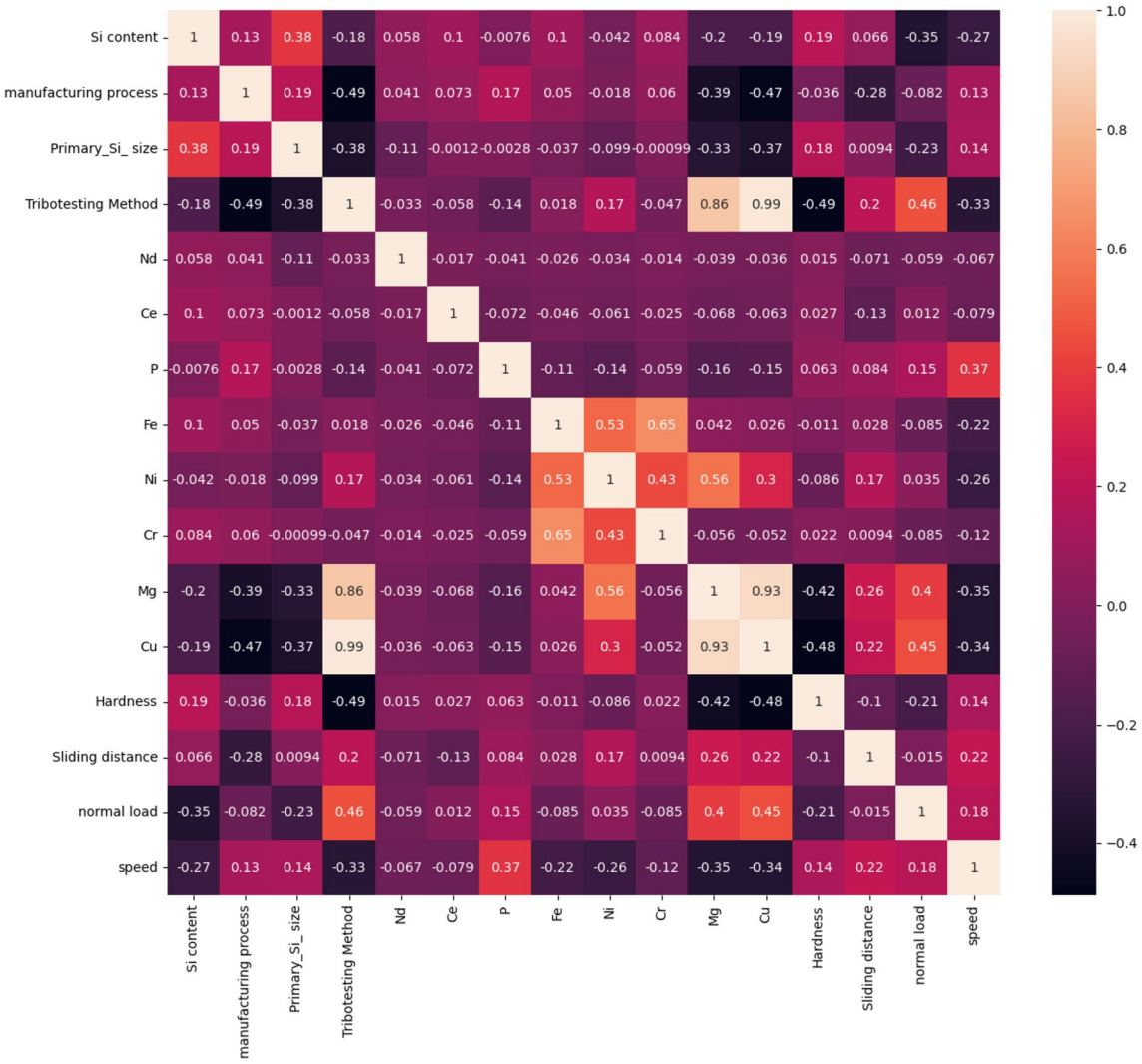

Fig. 8 Correlation coefficient matrix of input variables

The coefficient of determination, also known as the R2 score, is the most crucial performance metric to focus on when solving a supervised learning regression problem. The R2 score can vary between 0 to 1. When R2 is equal to zero, it implies that there is no correlation, and therefore the model is unable to explain the variation in the given dataset. If R2 is less than 0.5, it indicates that a weak correlation exists between the variables, and the ML model is regarded as being unable to accurately predict the output. The R2 value that falls anywhere between 0.70 and 0.9 suggests satisfactory performance, whereas a number that is more than 0.9 indicates extremely satisfactory execution of the model. When the R2 score is equal to 1, it denotes that the model fits the data perfectly, and it is able to accurately describe the variation in the data without making any errors. In addition to the R2 score, statistical measures are important metrics in deciding the model's accuracy. Thus, the performance of different models was evaluated by comparing wear rates obtained from experiments with predicted wear rates using three measures: the Mean Absolute Error (MAE), the Mean Squared Error (MSE), the Root Mean Squared Error (RMSE), and the Coefficient of Determination (R2). These metrics for regression analysis are defined as follows:

$$MAE = \frac{1}{m}\sum_{i=1}^{m} \left|\left(y_i - \hat{y}_i\right)\right|$$

$$MSE = \frac{1}{m}\sum_{i=1}^{m} \left(y_i - \hat{y}_i\right)^2$$

$$RMSE = \sqrt{\frac{1}{m}\sum_{i=1}^{m} \left(y_i - \hat{y}_i\right)^2}$$

where, m = number of experimental data, y_i = actual value, $\hat{y}_i$ = predicted value

Fig. 9 Correlation coefficient matrix after removing highly correlated variables

The parameters of the models were optimized using grid search and cross-validation (cv) technique to improve prediction (Table 2). SVR with hyperparameters, c = 10, gamma = 0.01 and kernel = rbf, shows the lowest R2 score. KNN which is based on the distance calculation method also underperformed as compared to other models. In KNN, n_neighbors was kept 4 where weights maintained as distance. For RF model, the best predictions are observed for max_features = 5, max_depth = 10 with n_estimators as 20. The random forest algorithm's better performance is due to the ensemble method consisting randomized decision trees. The R2 score achieved in the RF is 0.8846 with MAE = 0.168 MSE = 0.049, and RMSE = 0.222 respectively (Table 3).

It is interesting to note that tree-based machine learning models (RF, XGB, and DT) provided better outcomes as compared to high-order counterparts (SVR, ML). As the dataset is small and has relatively lower dimensions which is one of the many potential causes resulting in overfitting and inability for generalisation The most significant limitation of the tree-based approaches is the requirement of rebuilding and recalculation during updating the existing model with new data because this modification impacts all of the model's iterations.

3.5.2 RF Model Performance

The performance of different models has been evaluated by determining the R squared value (R2 score) for the

Table 2 Parametric optimization of different ML models

Model Name	Optimized parameters
RF	max_features = 5, max_depth = 10, n_estimators = 20
GB	learning_rate = 0.4, n_estimators = 50
SVR	c = 10, gamma = 0.01 and kernel = rbf
KNN	n_neighbors = 4, weights = distance
ANN	activation = relu, alpha = 0.001, hidden_layer_sizes = (50, 100, 50)

Table 3 Performance analysis of different models

Model Name	MAE	MSE	RMSE	R2
RF	0.168	0.049	0.222	0.8846
GB	0.200	0.072	0.265	0.8329
SVR	0.317	0.192	0.439	0.5507
KNN	0.239	0.113	0.336	0.7362
ANN	0.221	0.099	0.315	0.7402

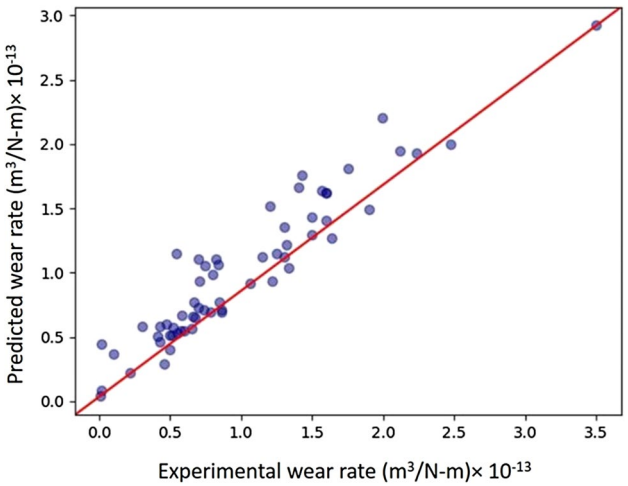

Fig. 10 Predicted wear rate vs actual wear rate in RF model

prediction of wear rate. The dataset has been split into two parts: 80% contains the training data and 20% contains the test data. Among the models, the R2 score is found to be maximum for the RF model.

The fitted model can predict the wear rate with a score of 88.46%. The comparison between the predicted wear rate and the actual wear rate obtained from experiments was then evaluated. It shows a good correlation exists between the predicted value and the actual values from Fig. 10. In addition, this model is able to determine the most important characteristics that influence the friction and wear of Al–20Si alloys by analyzing data obtained in different experiments. This knowledge can be put to good use in enhancing the synthesis process for Al–20Si alloys and locating the conditions under which production is at its most efficient.

3.5.3 Feature Importance of the Model

The feature importance analysis helps in determining the influence of different variables on the prediction. It has fractional values that vary between 0 to 1. A score near 1 indicates more influence in predicting the wear rate. The benefit of employing the gradient boost approach is that each attribute's relevance score can be determined rather quickly after the promotion tree is built. In general, the significance score assesses the importance of a feature in the model's raised decision tree construction. By repeatedly ranking each characteristic in the dataset, attribute importance is determined. The significance is calculated by increasing the number of performance metrics divided by each attribute, point in a single decision tree, and the node is in charge of the amount of records and weighting. Figure 11 shows the order of importance of the different input variables used in the model. It can be observed that normal load is the most important parameter followed by sliding distance and primary Si content.

In order to accurately estimate the wear rate, each of the independent factors had to have a score that is not zero. Figure 11 shows, the normal load, which is one of the tribological variables, received the highest score and made the most contribution to the overall equation representing wear rate prediction.

3.5.4 Worn Surface Analysis

The variation of normal load applied, which has been found as the most important feature from the model, plays an important role in the transformation from a mild form of wear into a severe form of wear. Figure 12 shows FESEM analysis of the worn surfaces to study the change in wear behaviour under 10 N and 25 N load at a sliding distance of 1000 m and sliding velocity of 1.5 m/s. The presence of grooves parallel to sliding directions indicates abrasive wear. However, the strong bonding of fine silicon particles resists the plastic deformation and delamination in case of friction stir processed alloy as shown in (Fig. 12d). This may be due to ploughing action by the hard silicon particles leading to abrasive wear. For friction stir processed samples, finer silicon particles have a better bonding with the matrix and thereby reducing the probability of microcracking underneath the surface. The abrasive grooves are narrower and less plastic deformation has occurred in the friction stir processed alloy than in the as-cast alloy. Under low and intermediate loading conditions, the wear mechanism is primarily governed by abrasive wear by hard silicon particles and possibly oxidative wear by the formation of mechanically mixed layer (MML).

Figure 13 shows the EDS analysis of the worn surace of the sample. It shows the presence iron (Fe), (O), silicon (Si), aluminium (Al) and carbon (C).It indicates iron oxieds coming from counterface material. The presence of Fe peak indicates the counterface material has been worn and the material is transferred. The wear of the counterface can be attributed to the hard silicon particles portruded from the sample surface. The friction between the two sliding surfaces results in increase in the temperature and reacts with O leading to the formation of oxides. Thus, oxides formed bythe iron from counter surace and matrix material together constitute MML to protects the tribosurface from further wear.

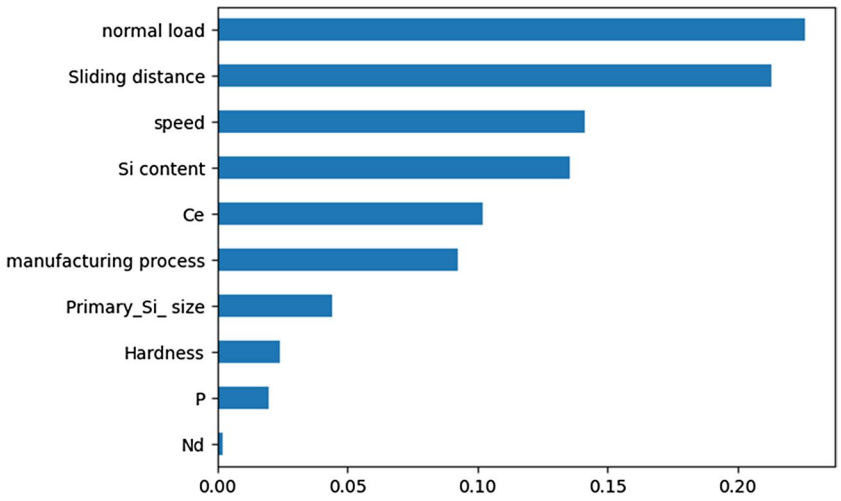

Fig. 11 Feature importance in RF model

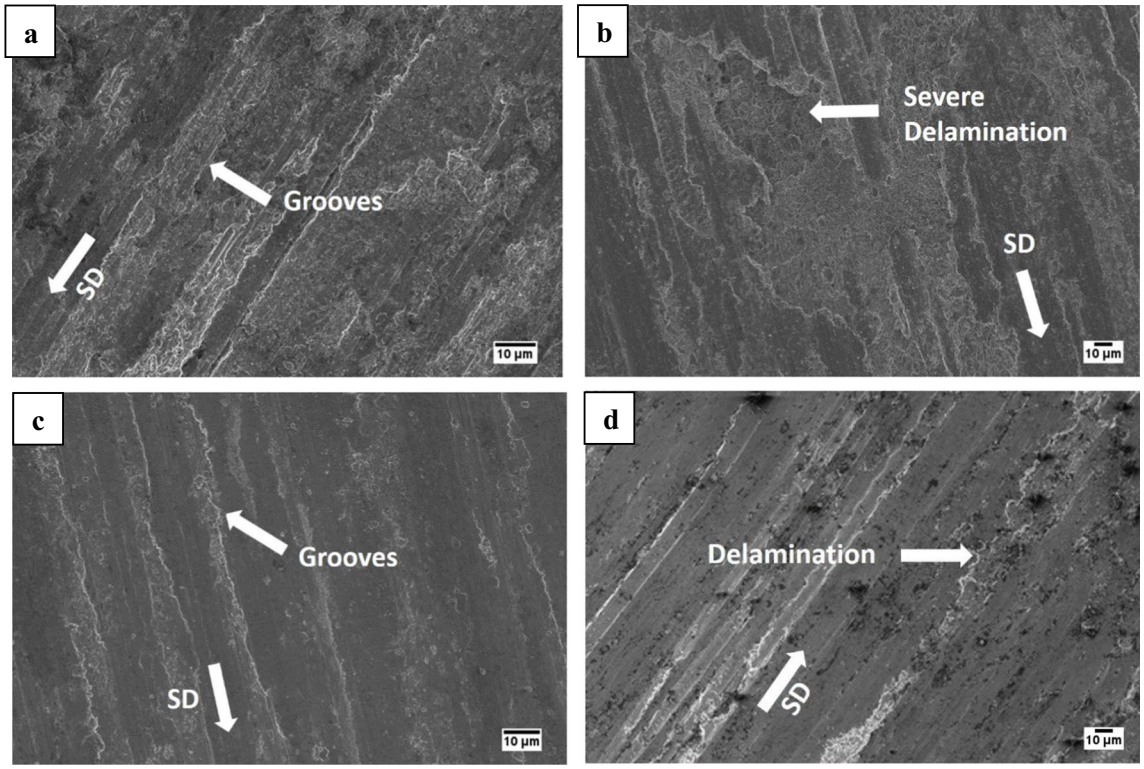

Fig. 12 Worn surface morphology of Al–20Si alloy at **a** as-cast at 10N **b** as-cast at 25N **c** FSP at 10N **d** FSP at 25N

On the other hand, at higher loading conditions, adhesive wear has the dominant role in the wear behaviour. Figure 12b shows severe delamination is observed in the as-cast Al–20Si alloy. The oxide layer is detached at higher load and considerable material removal occurs at a rapid rate during sliding contact of the tribo surfaces leading to delamination at higher loading conditions.

4 Conclusions

In the present study, Al–20Si alloy is fabricated through the liquid metallurgy route, and Friction stir processing is then applied to it. The microstructure of friction stir processed Al–20Si alloy was then investigated. In addition, the wear rates for those alloys were then determined and compared

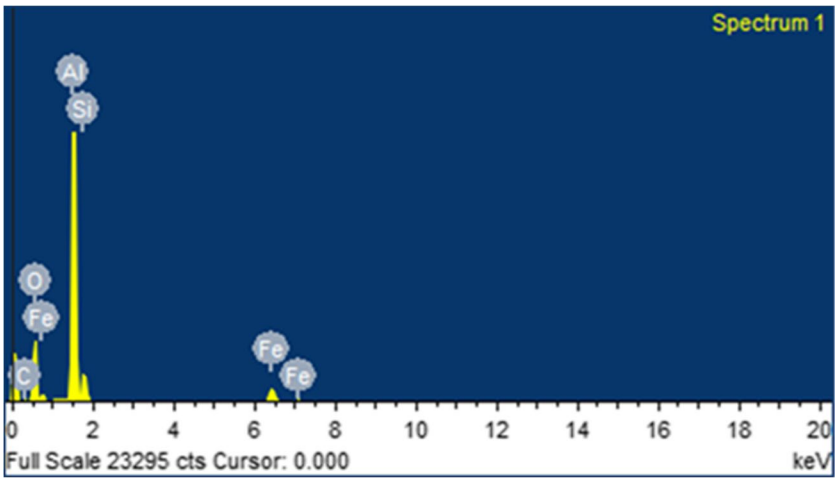

Fig. 13 EDS analysis of the worn surface friction stir processed Al–20Si alloy

with the values predicted in five different models of machine learning to find the best fit machine learning model. Further investigation can be carried out in this area by focusing on adding different refiners and varying tribological process variables in FSP or other related processes. The significant findings obtained are as follows:

- Microstructural analysis shows the significant refinement of primary Si and modification of eutectic silicon on the surface of friction stir processed Al–20Si alloy. The average size of primary Si reduced from 52.23 µm to 4.69 µm. Similarly, eutectic Si size decreased from 8.12 µm to 0.74 µm.
- The wear mechanism is based on the combination of abrasive, delamination, and oxidative wear. As Normal load is the most important factor, the mechanism changes with different loading conditions. When load is increased, the MML formed because of frictional heating. On further increase in load, the MML breaks and delamination wear occurs. Improved wear resistance is observed because of the microstructural refinement of primary Si and eutectic Si through the FSP route.
- The different models used for the prediction of wear rate performed well. However, Random Forest regression model performed the best on the dataset with an R2 value of 0.8846. Similarly, the MAE, MSE, and RMSE values are 0.168, 0.049, and 0.265 respectively.
- From the feature importance analysis, the normal load has the most significant contribution in predicting the wear rate using the RF model.

Acknowledgements The authors are thankful to IIT Bhubaneswar for providing experimental facilities.

Author Contributions All authors contributed to the study. Material preparation, data collection, original draft and analysis were performed by Mihira Acharya. conceptualization, design and review part were carried out by Dr. Animesh Mandal. All authors read and approved the final manuscript.

Funding The authors declare that no funds, grants, or other support were received during the preparation of this manuscript.

Data Availability The dataset used in the current study is available on reasonable request.

Declarations

Ethics Approval Not applicable.

Consent to Participate Not applicable.

Consent for Publication The authors have given consent for publication as per the journal policy.

Competing Interests The authors declare no competing interests.

References

1. Acharya M, Mandal A (2021) Effect of semi-solid heat treatment on the microstructure and dry sliding wear behavior of Al–20Si alloy at optimized parametric conditions. Met Mater Int 27:1578–1586. https://doi.org/10.1007/s12540-019-00550-6
2. Stojanovic B, Bukvic M, Epler I (2018) Application of aluminum and aluminum alloys in engineering. Appl Eng Lett 3:52–62. https://doi.org/10.18485/aeletters.2018.3.2.2
3. Bulei C, Stojanovic B, Utu D (2022) Developments of discontinuously reinforced aluminium matrix composites: Solving the needs for the matrix. J Phys Conf Ser 2212. https://doi.org/10.1088/1742-6596/2212/1/012029
4. Kapranos P, Kirkwood DH, Atkinson HV et al (2003) Thixoforming of an automotive part in A390 hypereutectic Al-Si alloy. J Mater Process Technol 135:271–277. https://doi.org/10.1016/S0924-0136(02)00857-9

5. Lee ES (2000) Study on the economics of hypereutectic aluminum-silicon (Al-Si) alloy machining. Int J Adv Manuf Technol 16:700–708. https://doi.org/10.1007/s001700070021
6. Zhao JW, Wu S Sen (2010) Microstructure and mechanical properties of rheo-diecasted A390 alloy. Trans Nonferrous Met Soc China (English Ed 20:s754–s757. https://doi.org/10.1016/S1003-6326(10)60576-6
7. Stojanović B, Gajević S, Kostić N et al (2022) Optimization of parameters that affect wear of A356/Al2O3 nanocomposites using RSM, ANN, GA and PSO methods. Ind Lubr Tribol 74:350–359. https://doi.org/10.1108/ILT-07-2021-0262
8. Stojanović B, Tomović R, Gajević S, Petrović J, Miladinović S (2022) Tribological Behavior of Aluminum Composites Using Taguchi Design and Ann. Adv Eng Lett 1:28–34. https://doi.org/10.46793/adeletters.2022.1.1.5
9. Milojević S, Stojanović B (2018) Determination of tribological properties of aluminum cylinder by application of Taguchi method and ANN-based model. J Brazilian Soc Mech Sci Eng 40. https://doi.org/10.1007/s40430-018-1495-8
10. Elmadagli M, Perry T, Alpas AT (2007) A parametric study of the relationship between microstructure and wear resistance of Al – Si alloys. Wear 262:79–92. https://doi.org/10.1016/j.wear.2006.03.043
11. Prasad BK, Venkateswarlu K, Modi OP et al (1998) Sliding wear behavior of some Al-Si alloys: role of shape and size of si particles and test conditions. Metall Mater Trans A Phys Metall Mater Sci 29:2747–2752. https://doi.org/10.1007/s11661-998-0315-7
12. Acharya M, Mandal A (2019) Individual and synergistic effect of gamma alumina (γ-Al2O3) and strontium on microstructure and mechanical properties of Al–20Si alloy. Trans Nonferrous Met Soc China 29:1353–1364. https://doi.org/10.1016/S1003-6326(19)65042-9
13. Shi WX, Gao B, Tu GF, Li SW (2010) Effect of Nd on microstructure and wear resistance of hypereutectic Al-20%Si alloy. J Alloys Compd 508:480–485. https://doi.org/10.1016/j.jallcom.2010.08.098
14. Stojanović B, Gajević S, Miloradović N et al (2023) Comparative analysis of hybrid composites based on a356 and Za-27 alloys regarding their tribological behaviour. Commun Sci Lett Univ Žilina 25:B215–B227. https://doi.org/10.26552/com.C.2023.056
15. Acharya M, Mondol S, Mandal A (2020) Development of high strength suction cast hypereutectic Al–20Si alloy containing gamma alumina and strontium. Mater Sci Technol (United Kingdom) 36. https://doi.org/10.1080/02670836.2020.1724403
16. Charandabi FK, Jafarian HR, Mahdavi S (2021) Modification of microstructure, hardness, and wear characteristics of an automotive-grade Al-Si alloy after friction stir processing. J Adhes Sci Technol 35:2696–2709. https://doi.org/10.1080/01694243.2021.1898858
17. Hasan S, Kordijazi A, Rohatgi PK, Nosonovsky M (2021) Modeling of dry friction and wear of aluminum base alloys using machine learning algorithms. Tribol Int 161:107065. https://doi.org/10.1016/j.triboint.2021.107065
18. Malamousi K, Delibasis K, Allcock B, Kamnis S (2022) Digital transformation of thermal and cold spray processes with emphasis on machine learning. Surf Coatings Technol 433:128138. https://doi.org/10.1016/j.surfcoat.2022.128138
19. Gyurova LA, Friedrich K (2011) Artificial neural networks for predicting sliding friction and wear properties of polyphenylene sulfide composites. Tribiology Int 44:603–609. https://doi.org/10.1016/j.triboint.2010.12.011
20. Graser J, Kauwe SK, Sparks TD (2018) Machine learning and energy minimization approaches for crystal structure predictions : a review and new horizons. Chem Mater 30:3601–3612. https://doi.org/10.1021/acs.chemmater.7b05304
21. Schmidt J (2019) Recent advances and applications of machine learning in solid- state materials science. npj Comput Mater 5:1–36. https://doi.org/10.1038/s41524-019-0221-0
22. Wen C, Zhang Y, Wang C et al (2019) Machine learning assisted design of high entropy alloys with desired property. Acta Mater 170:109–117
23. Chang Y, Jui C, Lee W (2019) Prediction of the composition and hardness of high-entropy alloys by machine learning. J Mater Sci 71:3433–3442
24. Hasan MS, Wong T, Rohatgi PK, Nosonovsky M (2022) Analysis of the friction and wear of graphene reinforced aluminum metal matrix composites using machine learning models. Tribol Int 170:107527. https://doi.org/10.1016/j.triboint.2022.107527
25. Canute KR, Ojha SSN, Microstructure WÁ (2012) Investigation on the wear properties of primary Si modified Al – 20Si alloy. Trans Indian Inst Met 65:673–676. https://doi.org/10.1007/s12666-012-0174-1
26. Yii SLJ, Anas NM, Ramdziah MN, Anasyida AS (2016) Microstructural and mechanical properties of Al-20%Si containing cerium. Procedia Chem 19:304–310. https://doi.org/10.1016/j.proche.2016.03.015
27. Tiwari K, Gautam G, Kumar N et al (2018) Effect of primary silicon refinement on mechanical and wear properties of a hypereutectic Al-Si alloy. Silicon 10:2227–2239. https://doi.org/10.1007/s12633-017-9755-2
28. Wang F, Liu H, Ma Y, Jin Y (2004) Effect of Si content on the dry sliding wear properties of spray-deposited Al – Si alloy. Mater Des 25:163–166. https://doi.org/10.1016/j.matdes.2003.08.005
29. Raghukiran N, Kumar R (2013) Processing and dry sliding wear performance of spray deposited hyper-eutectic aluminum – silicon alloys. J Mater Process Tech 213:401–410. https://doi.org/10.1016/j.jmatprotec.2012.10.007
30. Kaiser MS, Sabbir SH, Kabir MS et al (2018) Study of mechanical and wear behaviour of hyper-eutectic Al-Si automotive alloy through Fe, Ni and Cr addition. Mater Res 21:1–9. https://doi.org/10.1590/1980-5373-MR-2017-1096
31. Li Q, Zhu Y, Li B et al (2018) Effect of iron addition on the microstructures and properties of hypereutectic Al-20%Si alloys. Mater Res Express 6:016506–016516
32. Barekar NS, Dhindaw BK, Fan Z (2010) Improvement in silicon morphology and mechanical properties of Al–17Si alloy by melt conditioning shear technology. Int J Cast Met Res 23:225–231. https://doi.org/10.1179/136404610X12665088537338
33. Alshmri F, Atkinson HV, Hainsworth SV et al (2014) Dry sliding wear of aluminium-high silicon hypereutectic alloys. Wear 313:106–116. https://doi.org/10.1016/j.wear.2014.02.010
34. Al-samarai RA, Ahmad KR, Al-Douri Y (2012) Evaluate the effects of various surface roughness on the tribological characteristics under dry and lubricated conditions for Al–Si alloy. J Surf Eng Mater Adv Technol 2:167–173
35. Angadi BM, Reddy AC, Nehru J et al (2016) Effect of phosphorus addition on friction-interface temperature and wear behaviour of hypereutectic Al–Si alloys. Indian Foundry J 62:56–66
36. Jasim KM, Dwarakadasa ES (1992) Dry sliding wear in binary Al–Si alloys at low bearing pressures. J Mater Sci Lett 11:421–423
37. Mahmoud TS (2013) Surface modification of A390 hypereutectic Al–Si cast alloys using friction stir processing. Surf Coat Technol 228:209–220. https://doi.org/10.1016/j.surfcoat.2013.04.031
38. Xu CL, Yang YF, Wang HY, Jiang QC (2007) Effects of modification and heat-treatment on the abrasive wear behavior of hypereutectic Al-Si alloys. J Mater Sci 42:6331–6338. https://doi.org/10.1007/s10853-006-1189-y

39. Vijeesh V, Prabhu KN (2014) Review of microstructure evolution in hypereutectic Al-Si alloys and its effect on wear properties. Trans Indian Inst Met 67:1–18
40. Hao Y, Gao B, Tu GF et al (2011) Influence of high current pulsed electron beam (HCPEB) treatment on wear resistance of hypereutectic Al-17.5Si and Al-20Si alloys. Mater Sci Forum 675–677:693–696. https://doi.org/10.4028/www.scientific.net/MSF.675-677.693
41. Raju K, Harsha AP, Ojha SN (2010) Microstructural features, wear, and corrosion behaviour of spray cast Al – Si alloys. J Eng Tribol 225:151–160. https://doi.org/10.1177/2041305X10394055
42. Goudar DM, Magalad VT, Kurahatti RV (2020) Study of microstructure and tribological behaviour of spray cast high silicon hypereutectic Al-Si alloy. Adv Mater Process Technol 8:1245–1254. https://doi.org/10.1080/2374068X.2020.1855402
43. Okfalisa, Gazalba I, Mustakim, Reza NGI (2018) Comparative analysis of k-nearest neighbor and modified k-nearest neighbor algorithm for data classification. Proc - 2017 2nd Int Conf Inf Technol Inf Syst Electr Eng ICITISEE 2017 2018-Janua:294–298. https://doi.org/10.1109/ICITISEE.2017.8285514
44. Farahnakian F, Pahikkala T, Liljeberg P, Plosila J (2013) Energy aware consolidation algorithm based on K-nearest neighbor regression for cloud data centers. Proc - 2013 IEEE/ACM 6th Int Conf Util Cloud Comput UCC 2013 256–259. https://doi.org/10.1109/UCC.2013.51
45. Lian Z, Li M, Lu W (2022) Fatigue life prediction of aluminum alloy via knowledge-based machine learning. Int J Fatigue 157:106716. https://doi.org/10.1016/j.ijfatigue.2021.106716
46. Aydin F, Durgut R, Mustu M, Demir B (2023) Prediction of wear performance of ZK60 / CeO2 composites using machine learning models. Tribol Int 177:107945. https://doi.org/10.1016/j.triboint.2022.107945
47. Ma ZY (2008) Friction stir processing technology : a review. Metall Mater Trans A 39:642–658. https://doi.org/10.1007/s11661-007-9459-0
48. Mishra RS, Ma ZY (2005) Friction stir welding and processing. Mater Sci Eng R 50:1–78. https://doi.org/10.1016/j.mser.2005.07.001
49. Kliauga AM, Ferrante M (2005) Liquid formation and microstructural evolution during re-heating and partial melting of an extruded A356 aluminium alloy. Acta Mater 53:345–356. https://doi.org/10.1016/j.actamat.2004.09.030
50. Humphreys FJ, Ardakani MG (1994) The deformation of particle-containing aluminium single crystals. Acta Metall Mater 42:749–761